Chinese Journal of Natural Medicines

Reynosin protects neuronal cells from microglial neuroinflammation by suppressing NLRP3 inflammasome activation mediated by NADPH oxidase

Yanqiu YANG, Yue CHE, Mingxia FANG, Xiaohu YAO, Di ZHOU, Feng WANG, Gang CHEN, Dong LIANG, Ning LI, Yue HOU

Citation: Yanqiu YANG, Yue CHE, Mingxia FANG, Xiaohu YAO, Di ZHOU, Feng WANG, Gang CHEN, Dong LIANG, Ning LI, Yue HOU, Reynosin protects neuronal cells from microglial neuroinflammation by suppressing NLRP3 inflammasome activation mediated by NADPH oxidase, Chinese Journal of Natural Medicines, 2024, 22(6), 486−500. doi: 10.1016/S1875−5364(24)60652−7.

View online: https://doi.org/10.1016/S1875−5364(24)60652−7

Available online at www.sciencedirect.com
ScienceDirect
Chinese Journal of Natural Medicines 2024, **22**(6): 486-500
doi: 10.1016/S1875-5364(24)60652-7
Chinese Journal of Natural Medicines

•Original article•

Reynosin protects neuronal cells from microglial neuroinflammation by suppressing NLRP3 inflammasome activation mediated by NADPH oxidase

YANG Yanqiu[1, 2], CHE Yue[1, 2], FANG Mingxia[1, 2], YAO Xiaohu[1, 2], ZHOU Di[3], WANG Feng[1], CHEN Gang[3], LIANG Dong[4], LI Ning[3*], HOU Yue[1, 2*]

[1] *Key Laboratory of Bioresource Research and Development of Liaoning Province, College of Life and Health Sciences, Northeastern University, Shenyang 110000, China;*
[2] *National Frontiers Science Center for Industrial Intelligence and Systems Optimization, Key Laboratory of Data Analytics and Optimization for Smart Industry, Ministry of Education, Northeastern University, Shenyang 110000, China;*
[3] *School of Traditional Chinese Materia Medica, Key Laboratory of Innovative Traditional Chinese Medicine for Major Chronic Diseases of Liaoning province, Key Laboratory for TCM Material Basis Study and Innovative Drug Development of Shenyang City, Shenyang Pharmaceutical University, Shenyang 110000, China;*
[4] *State Key Laboratory for Chemistry and Molecular Engineering of Medicinal Resources, School of Chemistry and Pharmaceutical Sciences, Guangxi Normal University, Guilin 541000, China*

Available online 20 Jun., 2024

[ABSTRACT] Neuroinflammation, mediated by the nucleotide-binding oligomerization domain-like receptor family pyrin domain-containing-3 (NLRP3) inflammasome, is a significant contributor to the pathogenesis of neurodegenerative diseases (NDDs). Reynosin, a natural sesquiterpene lactone (SL), exhibits a broad spectrum of pharmacological effects, suggesting its potential therapeutic value. However, the effects and mechanism of reynosin on neuroinflammation remain elusive. The current study explores the effects and mechanisms of reynosin on neuroinflammation using mice and BV-2 microglial cells treated with lipopolysaccharide (LPS). Our findings reveal that reynosin effectively reduces microglial inflammation *in vitro*, as demonstrated by decreased CD11b expression and lowered interleukin-1 beta (IL-1β) and interleukin-18 (IL-18) mRNA and protein levels. Correspondingly, *in vivo*, results showed a reduction in the number of Iba-1 positive cells and alleviation of morphological alterations, alongside decreased expressions of IL-1β and IL-18. Further analysis indicates that reynosin inhibits NLRP3 inflammasome activation, evidenced by reduced transcription of NLRP3 and caspase-1, diminished NLRP3 protein expression, inhibited apoptosis-associated speck-like protein containing a CARD (ASC) oligomerization, and decreased caspase-1 self-cleavage. Additionally, reynosin curtailed the activation of nicotinamide adenine dinucleotide phosphate (NADPH) oxidase, demonstrated by reduced $NADP^+$ and NADPH levels, downregulation of $gp91^{phox}$ mRNA, protein expression, suppression of $p47^{phox}$ expression and translocation to the membrane. Moreover, reynosin exhibited a neuroprotective effect against microglial inflammation *in vivo* and *in vitro*. These collective findings underscore reynosin's capacity to mitigate microglial inflammation by inhibiting the NLRP3 inflammasome, thus highlighting its potential as a therapeutic agent for managing neuroinflammation.

[KEY WORDS] Microglia; NLRP3 inflammasome; Reactive oxygen species; NADPH oxidase; Neuron; Reynosin
[CLC Number] R965 **[Document code]** A **[Article ID]** 2095-6975(2024)06-0486-15

Introduction

Neurodegenerative diseases (NDDs) are commonly observed in the elderly population over 60 years old [1] and are characterized by progressive cognitive impairments and behavioral problems [2]. Research increasingly links these symptoms to the progressive degeneration and substantial loss of functional neurons [3, 4]. The underlying pathological processes of these disorders are diverse and complex, with neuroinflammation widely recognized as a key contributor to the progression of NDDs [4, 5]. This process triggers the overactivation of macrophage cells [6], infiltration of immune

[Received on] 20-Nov.-2023
[Research funding] This work is supported by the National Natural Science Foundation of China (No. 82174076), the Construction Project of Liaoning Provincial Key Laboratory, China (No. 2022JH13/10200026), the Fundamental Research Funds for the Central Universities (No. N2220002), the 111 Project (No. B16009), Scientific Research Fund of Liaoning Province Education Department (No. LJKZ0945), and Natural Science Foundation of Liaoning Province (No. 2022-MS-242).
[*]**Corresponding author]** E-mails: houyue@mail.neu.edu.cn (HOU Yue); liningsypharm@163.com (LI Ning)
These authors have no conflict of interest to declare.

cells [7], and excessive generations of pro-inflammatory mediators, such as cytokines, chemokines, and reactive oxygen species (ROS) [5], which ultimately lead to neuronal dysfunction and death [8]. Therapies targeting neuroinflammation have been shown to ameliorate cognitive impairments [9], with promising results observed in the clinical management of NDDs [10].

The nucleotide-binding oligomerization domain-like receptor family pyrin domain-containing-3 (NLRP3) inflammasome serves as a defensive response of the host against both endogenous and exogenous stimuli [11, 12], and its activation is tightly regulated. During activation, the components of the NLRP3 inflammasome, which include NLRP3, apoptosis-associated speck-like protein containing a C-terminal caspase recruitment domain (ASC), and caspase-1, become upregulated, oligomerize, and interact to form a multiprotein complex with bioactivity [13, 14]. This complex ultimately promotes the proteolytic generation of interleukin-1 beta (IL-1β) and interleukin-18 (IL-18), playing roles in neuroinflammation and pyroptosis [12, 15]. Numerous studies have demonstrated that the activation of the NLRP3 inflammasome contributes to the pathologies of NDDs [16]. The elevated expressions of its components, caspase-1 activation, and increased levels of IL-1β and IL-18 have been detected in animal models of Alzheimer's disease (AD) [17, 18]. Furthermore, the genetic ablation of NLRP3 and caspase-1 has been shown to suppress neuroinflammatory responses and alleviate spatial memory impairment in AD model animals [18], highlighting the significant therapeutic potential of inhibiting the NLRP3 inflammasome in the treatment of AD.

The role of nicotinamide adenine dinucleotide phosphate (NADPH) oxidase as a principal regulator of NLRP3 inflammasome activation is well-documented, with emerging studies continuing to elucidate its mechanisms [19]. Upon activation by various signals, NADPH oxidase generates superoxide ($O_2^{\cdot-}$), which is subsequently converted into hydrogen peroxide (H_2O_2) and ROS [20]. Previous research has demonstrated that NADPH oxidase facilitates the activation of the NLRP3 inflammasome by releasing ROS [21, 22]. Inhibiting NADPH oxidase has been shown to suppress inflammasome assembly and activity and reduce caspase-1 activation and IL-1β production and secretion [22]. Additionally, reducing NADPH oxidase activity has been found to improve memory function in animal models of AD [23]. Thus, targeting NADPH oxidase inhibition offers significant potential for mitigating neuroinflammation mediated by NLRP3 inflammasome activation and improving cognitive impairments.

Sesquiterpene lactones (SLs) are a class of natural compounds in Asteraceae plants [24]. Recently, SLs have garnered considerable attention due to their diverse pharmacological properties. Among these compounds, reynosin (Fig.1A), a natural SL, is found in the medicine-food homology plant *Laurus nobilis* L. [25] and the medicinal plants *Inula montana* L. [26] and *Costus speciosus* Smith [27]. Previous studies have demonstrated that reynosin possesses multiple pharmacological activities, including hepatoprotection [28], antioxidant stress mitigation [29], and neuroprotection [30]. Additionally, it has shown potent anti-inflammatory effects, evidenced by the significant inhibition of pro-inflammatory cytokine release *in vitro* [25, 27]. Given these notable pharmacological benefits, reynosin is increasingly recognized as a promising therapeutic candidate for the treatment of NDDs. However, the literature on the effects of reynosin on neuroinflammation is scant. Therefore, this study aims to investigate whether reynosin can protect neuronal cells against microglia-mediated neuroinflammation both *in vivo* and *in vitro* and to explore the underlying mechanisms associated with NLRP3 inflammasome involvement.

Material and Methods

Animal model, drugs, and grouping

Neuroinflammation was experimentally induced in adult C57BL/6 mice *via* intracerebroventricular (i.c.v.) injection of LPS (L2630; Sigma; St. Louis, MO, USA). Mice were anesthetized using 2.5% tribromoethanol (i.p) and received injections of LPS (2 μL, 20 mg·mL^{-1}) into the right hemisphere ventricle using stereotaxic coordinates (AP: −0.5 mm relative to the bregma, ML: 1.1 mm lateral to the sagittal suture, DV: −3.0 mm depth from the skull surface). The LPS was administered at a rate of 1 μL·min^{-1}, and the needle remained in place for an additional 5 min following the injection to prevent backflow. All infusion procedures were conducted 30 min prior to treatment each day. Control group received isovolumetric injections of 0.9% saline.

The animal experiments were conducted with the approval of the Animal and Medical Ethics Committee of Northeastern University (No. EC-2021A027). Reynosin, with high-performance liquid chromatography (HPLC) purity exceeding 98%, was isolated from the petroleum ether extract of *Michelia macclurei* Dandy roots. Minocycline hydrochloride (MINO, purity > 98%) was sourced from Meilunbio (Dalian, China). The mice were assigned into the following groups (n = 8/group): (1) vehicle group; (2) LPS group; (3) LPS + reynosin group (administered in doses of 2.5 mg·kg^{-1} and 5 mg·kg^{-1}); (4) LPS + MINO group (used as a positive control; 40 mg·kg^{-1}).

Immunofluorescence (IF) staining assay

IF staining assay was conducted to quantify the expressions of neuronal nuclei (NeuN), ionized calcium-binding adapter molecule 1 (Iba-1), and p47^{phox} in brain sections [31]. Briefly, coronal sections (10 μm thick) were harvested and incubated overnight at 4 °C with primary antibodies against Iba-1 (ab177847, Abcam, Cambridge, MA, USA; dilution 1 ∶ 500), NeuN (ab177487, Abcam, Cambridge, MA, USA; dilution 1 ∶ 1000), IL-18 (#67775, Cell Signaling Technology (CST); Danvers, MA, USA; dilution 1 ∶ 400) and p47^{phox} (ab166930, Abcam, Cambridge, MA, USA; dilution 1 ∶ 500). Following primary antibody incubation, sections were exposed to secondary antibodies conjugated with either fluorescein isothiocyanate (FITC, ab6717, Abcam, Cam-

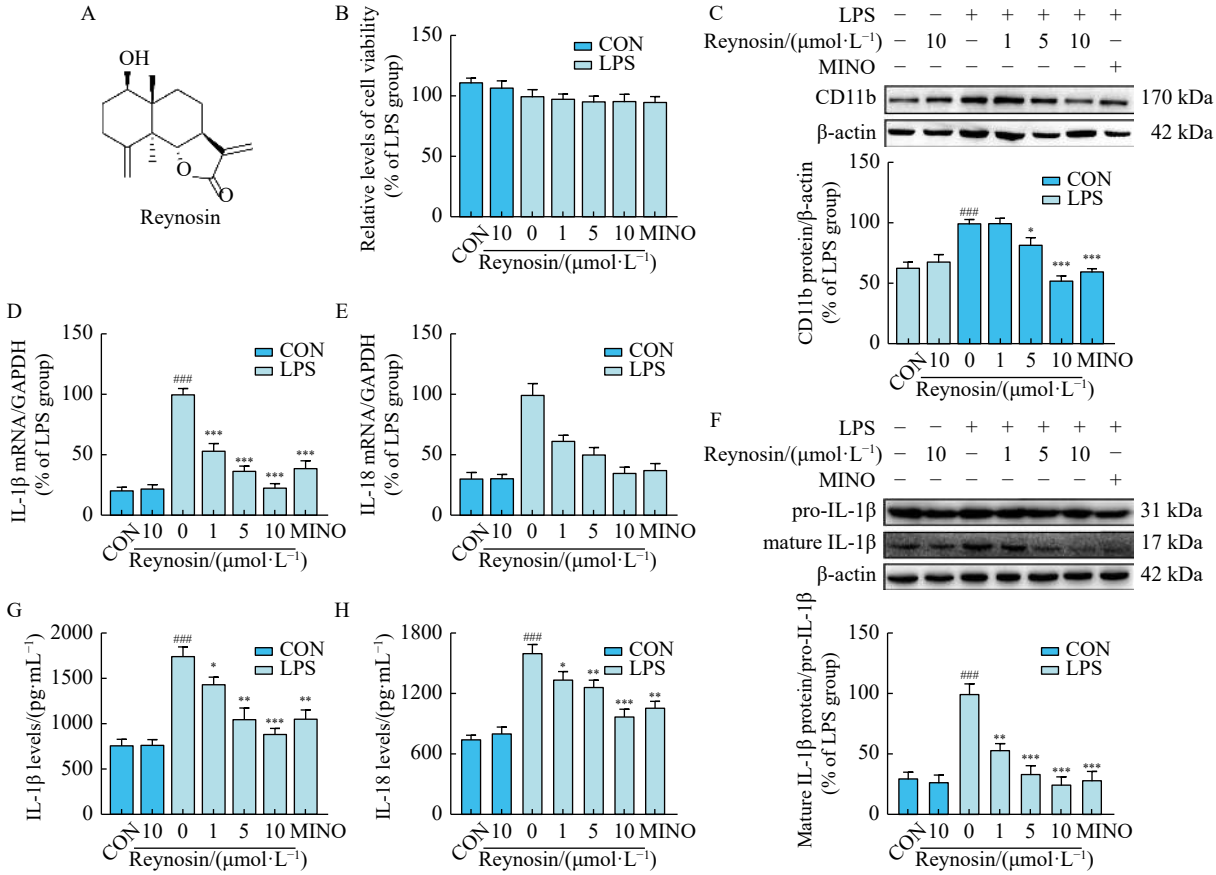

Fig. 1 Reynosin alleviated LPS-activated microglial inflammation *in vitro*. (A) Chemical structure of reynosin. BV-2 cells were subjected to LPS treatment to trigger neuroinflammation *in vitro*. (B) Cellular viability was measured by MTT assay, $n = 3$. The protein expressions of CD11b and IL-1β were evaluated by Western blotting. Representative images and statistical analysis of CD11b (C) and IL-1β (F) are shown, $n = 3$. (D–E, G–H) The mRNA and supernatant protein levels of IL-1β and IL-18 were detected using RT-PCR and ELISA commercial kits, respectively, $n = 3$. Data are expressed as mean ± SEM. $^{###}P < 0.001$ *vs* the CON group; $^{*}P < 0.05$, $^{**}P < 0.01$ and $^{***}P < 0.001$ *vs* the LPS group. MINO: minocycline hydrochloride (30 μmol·L^{-1}).

bridge, MA, USA; dilution 1 : 800) and CoraLite 594 (SA00013-4, Proteintech, Wuhan, China) for visualization. The stained sections from the cerebral cortex were imaged and analyzed using appropriate fluorescence microscopy techniques.

For the *in vitro* analysis of p47^{phox} and ASC expression, BV-2 microglial cells were fixed in 4% paraformaldehyde (PFA) and permeabilized with 0.02% Tween-20. Cells were then blocked using a 3% bovine serum albumin (BSA) buffer and incubated with primary antibodies specific to p47^{phox} or ASC for 24 h at 4 °C. Post-primary antibody incubation, cells were rinsed with PBS and incubated with secondary antibodies tagged with CoraLite 594 or FITC for 4 h in the darkness to prevent photobleaching. Fluorescence images were captured using a confocal microscope, ensuring consistency in exposure and magnification settings across all samples.

Cells, treatment, and (3-[4,5-dimethylthiazol-2-yl]-2,5-diphenyltetrazolium bromide (MTT) assay

BV-2 microglial cells and SH-SY5Y neuroblastoma cells were sourced from the School of Pharmacy, Nankai University (Tianjin, China) and American Type Culture Collection (ATCC, Houston, TX, USA), respectively. For the *in vitro* experiments, BV-2 cells were divided into several groups: control, reynosin-treated, lipopolysaccharide (LPS)-treated, LPS plus various concentrations of reynosin (1, 5, 10 μmol·L^{-1}), group and LPS plus minocycline hydrochloride (MINO). Cells were seeded and allowed to adhere for 12 h. Following a 2-hour pre-treatment with either reynosin or MINO, cells were co-incubated with LPS for an additional 24 h.

Cell viability was assessed using the MTT assay. BV-2 cells and SH-SY5Y cells were treated with MTT (Sigma; St. Louis, MO, USA) for 4 h. Post-incubation, the supernatants were removed, and cells were solubilized in dimethyl sulfoxide (DMSO). The absorbance was measured at 490 nm using a spectrophotometer. Relative cell viability was calculated based on these absorbance values, comparing treated cells to control groups to determine the cytotoxic or protective effects of the treatments.

Real-time reverse transcription-polymerase chain reaction (RT-PCR)

RNA samples were extracted from mouse cortex tissue and BV-2 cells utilizing the RNAiso reagent (Takara, Beijing, China). Two micrograms of RNA from each sample were re-

verse-transcribed into complementary DNA (cDNA) using the GoScript™ Reverse Transcription System (Promega; Madison, WI, USA). Primers for the target genes were designed and synthesized by Sangon Biotech (Shanghai, China), with sequences detailed in Table 1. Quantitative real-time PCR (RT-PCR) was conducted using the GoTaq® qPCR Master Mix (Promega; Madison, WI, USA). Glyceraldehyde 3-phosphate dehydrogenase (GAPDH) served as the internal control to ensure normalization and accuracy of the expression data.

Western blotting assay

Protein samples from mouse cortex tissues and BV-2 cells were prepared by homogenizing in RIPA lysis buffer containing 1% Trition-100, 1% deoxycholate, 0.1% sodium dodecyl sulfate (SDS), and 1 mmol·L^{-1} phenylmethylsulfonyl fluoride (PMSF). The homogenates were lysed on ice for 1 hour, followed by centrifugation at 12 000 × g for 15 min. The supernatants were then subjected to heat denaturation at 70 °C for 10 min. Protein concentrations were determined using the bicinchoninic acid (BCA) assay. For protein analysis, 30 μg of each sample was separated by 12% SDS-polyacrylamide gel electrophoresis (PAGE) and subsequently transferred to polyvinylidene difluoride (PVDF) membranes (Millipore, Bedford, MA, USA). The membranes were blocked with 5% skim milk for 30 min, and incubated overnight at 4 °C with primary antibodies targeting CD11b (#49420; CST; Danvers, MA, USA), IL-1β (#12242; CST; Danvers, MA, USA), NLRP3 (#15101; CST; Danvers, MA, USA), caspase-1 (ab179515; Abcam; Cambridge, MA, USA), gp91^{phox} (ab129068; Abcam; Cambridge, MA, USA), β-actin (66009-1; Proteintech; Wuhan, China) and GAPDH (#8884; CST; Danvers, MA, USA). After incubation with primary antibodies, the membranes were washed three times with TBST buffer and incubated with horseradish peroxidase (HRP)-conjugated secondary antibodies (SA00001-2; Proteintech, Wuhan, China) for 4 h. The protein bands were visualized and documented. β-actin or GAPDH was used as an internal control to ensure equal protein loading and transfer across all samples.

Enzyme-linked immunosorbent assay (ELISA)

The concentrations of IL-1β and IL-18 were quantified using commercial ELISA kits, following the manufacturer's instructions. The IL-1β ELISA kit (MLB00C) was sourced from NOVUS (Shanghai, China), and the IL-18 kit (EK0433) was obtained from Boster (Wuhan, China). Both IL-1β and IL-18 levels were determined based on standard curves provided with the kits. The results were expressed in picograms per milliliter of supernatant, facilitating accurate and reproducible measurement of cytokine levels in the samples.

ROS measurement

The levels of ROS, both *in vivo* and *in vitro*, were quantified using four independent assays. These included dihydroethidium (DHE) staining, sourced from Beyotime (Shanghai, China), a commercial hydrogen peroxide (H_2O_2) kit also from Beyotime (Shanghai, China), the Amplex Red H_2O_2 assay provided by Invitrogen (Carlsbad, CA, USA), and the 2′,7′-dichlorofluorescein diacetate (H2DCF-DA) assay from Nanjing Jiancheng (Nanjing, China). Each assay was selected for its specificity and sensitivity in detecting different forms of ROS within biological samples.

DHE staining: As previously described [32, 33], the DHE staining method was utilized both *in vivo* and *in vitro* to detect ROS. *In vivo,* mice were intraperitoneally injected with a DHE probe at a dosage of 20 mg·kg^{-1}. Following a 2-hour incubation, brain tissues were harvested, fixed, and dehydrated to prepare sections for imaging. *In vitro,* BV-2 cells were washed and incubated with a 10 μmol·L^{-1} concentration of the DHE probe at 37°C for 1 hour in darkness. The stained cells and tissues were visualized and imaged for further analysis.

H_2O_2 measurement: Cortex tissues were weighted and homogenized in lysis buffer on ice. After centrifugation at 12 000 × g for 5 min, the supernatants were collected, and protein concentrations were determined using the BCA method. Samples were then mixed with reagents from the commercial hydrogen peroxide kit (Beyotime, Shanghai, China) and processed for 30 min. Absorbance was measured at a wavelength of 560 nm, and H_2O_2 content was calculated and expressed in micromoles per gram of protein.

Amplex red assay: For *in vitro* H_2O_2 level measurement, the Amplex Red assay was performed according to the kit's instructions (Invitrogen, Carlsbad, CA, USA). BV-2 cells were washed with PBS and incubated with a buffer containing 10 μmol·L^{-1} Amplex Red and 0.2 U·mL^{-1} HRP for 1 h at 37 °C. Fluorescence was measured with 485/595) excitation at 485 nm and emission at 595 nm. Relative fluorescence

Table 1 Primer sequences of target genes used for real-time PCR

Gene bank number	Gene	Forward primer (5′-3′)	Reverse primer (5′-3′)	Primer size
NM_008361	*IL-1β*	TGACGGACCCCAAAAGATGA	TCTCCACAGCCACAATGAGT	20 bp (F), 20 bp (R)
NM_001357221	*IL-18*	ACAACTTTGGCCGACTTCAC	GGTCACAGCCAGTCCTCTTA	20 bp (F), 20 bp (R)
NM_001359638	*NLRP3*	CGAGATGCAGGAGGAAGACT	CCTTGGGCGAGTTGTGAAAA	20 bp (F), 20 bp (R)
NM_009807	*caspase-1*	TGTCAGGGGCTCACTTTTCA	CCGGGAAGAGGTAGAAACGT	20 bp (F), 20 bp (R)
NM_007807	*gp91phox*	GGTTTTGGCGATCTCAGCAA	ACTGTCCCACCTCCATCTTG	20 bp (F), 19bp (R)
NM_001289726	*GAPDH*	AGGTCGGTGTGAACGGATTTG	TGTAGACCATGTAGTTGAGGTCA	21bp (F), 22 bp (R)

units (RFU) were then calculated.

H2DCFDA assay: Fresh cortex tissues were rinsed with chilled saline and digested with 0.25% trypsin, with gentle agitation. The resultant cell suspensions were collected by centrifugation at 500 × g for 10 min to obtain single-cell suspensions. These cells, along with BV-2 cells, were seeded and incubated with a 20 μmol·L^{-1} H2DCF-DA probe for 1 h in darkness. Fluorescence was recorded (E_X/E_m =485/525), and RFU was computed accordingly.

Intracellular NADP$^+$ and NADPH quantification

Intracellular NADP$^+$ and NADPH levels in cortex tissues and BV-2 cells were determined using a commercial NADP$^+$/NADPH assay kit (Beyotime, Shanghai, China). The tissues and cells were homogenized with the provided extraction reagent and lysed on ice. The supernatants were collected following centrifugation at 12 000 × g for 15 min, and the protein concentrations were quantitatively analyzed using the BCA method. Following the manufacturer's protocol, the samples were reacted with the assay reagents. Absorbance was measured at 450 nm. The concentrations of NADP$^+$ and NADPH were calculated and expressed as a percentage of the control, normalized per gram of protein.

Neurotoxicity determination

To assess neurotoxicity, a conditioned medium (CM) culture model was utilized with SH-SY5Y neuronal cells. BV-2 cells were seeded and treated with LPS. Following treatment, supernatants were collected, centrifuged at 1 000 × g for 15 min at 4 °C, and used as the CM. SH-SY5Y cells were then seeded and incubated with either a normal medium or the collected CMs for 48 hours to evaluate the effects on neuronal viability.

MTT Assay

Cell viability was measured using the MTT assay, which assesses the metabolic activity of the cells.

Lactate Dehydrogenase (LDH) release assay: LDH release, indicative of cell membrane integrity and cytotoxicity, was quantified using a commercial kit (Beyotime, Shanghai, China). SH-SY5Y cells were treated with either serum-free DMEM or CMs, followed by incubation with LDH release reagent for 1 h in the dark. After centrifugation at 400 × g for 5 min, supernatants were collected and reacted with the kit's reagents under dark conditions. The absorbance at 490 nm was measured, and relative LDH levels were calculated.

Calcein AM/Propidium Iodide (PI) staining: For further evaluation of cell viability and death, cells were washed with PBS, and stained with calcein AM and PI (10 μmol·L^{-1}, Beyotime; Shanghai, China) for 45 min in the dark. Calcein AM stains live cells green, while PI stains dead cells red. Images were taken, analyzed, and documented to assess the proportion of live versus dead cells.

Statistical analysis

All experimental data are presented as mean ± SEM. To determine statistical significance among different groups, a one-way analysis of variance (ANOVA) was employed, followed by Tukey's post hoc test for multiple comparisons. Statistical significance was established at a threshold of $P < 0.05$.

Results

Reynosin suppresses LPS-induced microglial inflammation responses in vitro

To investigate the anti-neuroinflammatory effect of reynosin, BV-2 microglial cells were stimulated with LPS to mimic microglial activation *in vitro*. Initial assessments using the MTT assay indicated that reynosin (at concentrations of 1, 5, and 10 μmol·L^{-1}) did not significantly affect cell viability, a finding also observed in cells treated with MINO (Fig. 1B). Further analysis revealed that reynosin effectively reduced the expression of the microglial activation marker CD11b (Fig. 1C). It also inhibited the mRNA levels of pro-inflammatory cytokines IL-1β and IL-18 (Figs. 1D–1E), as well as the expression of mature IL-1β protein (Fig. 1F). Additionally, reynosin decreased the levels of IL-1β and IL-18 protein in the supernatant (Figs. 1G–1H), demonstrating a suppression of inflammatory mediators typically upregulated by LPS. The level of inhibition observed was comparable to that achieved with MINO treatment. These findings confirm that reynosin effectively suppresses microglial inflammatory responses *in vitro*.

Reynosin suppresses LPS-induced microglial inflammation responses in vivo

To determine whether reynosin could mitigate neuroinflammation mediated by microglia *in vitro,* mice were intracerebroventricularly (i.c.v.) injected with LPS, and microglial activation was subsequently assessed. Following LPS administration, there was a significant increase in microglial activation as evidenced by the elevated number of Iba-1 positive cells and the morphological transition from a resting state with small cell bodies and few, short branches to an activated state characterized by enlarged cell bodies and numerous, elongated branches (Figs. 2A–2B). This morphological change is indicative of microglial activation. Concomitantly, there was a notable increase in the expression of pro-inflammatory cytokines. Both mRNA and protein levels of IL-1β and IL-18 were significantly elevated in LPS-administered mice compared with those treated with the vehicle control (Figs. 2C–2H). As illustrated in Figs. 2A–2B, Treatment with reynosin at doses of 2.5 and 5 mg·kg^{-1} effectively reduced these markers of microglial activation and inflammation. Specifically, reynosin significantly lowered IL-1β and IL-18 mRNA levels (Figs. 2C–2D) and decreased their protein expression and relative fluorescence intensity (Figs. 2E–2I). MINO, used as a positive control, similarly reduced microglial activation (Figs. 2A–2B) and decreased the expression of both IL-1β and IL-18 mRNA and proteins (Figs. 2C–2I). These findings suggest that reynosin, like MINO, effectively inhibits LPS-induced microglial inflammation *in vivo.*

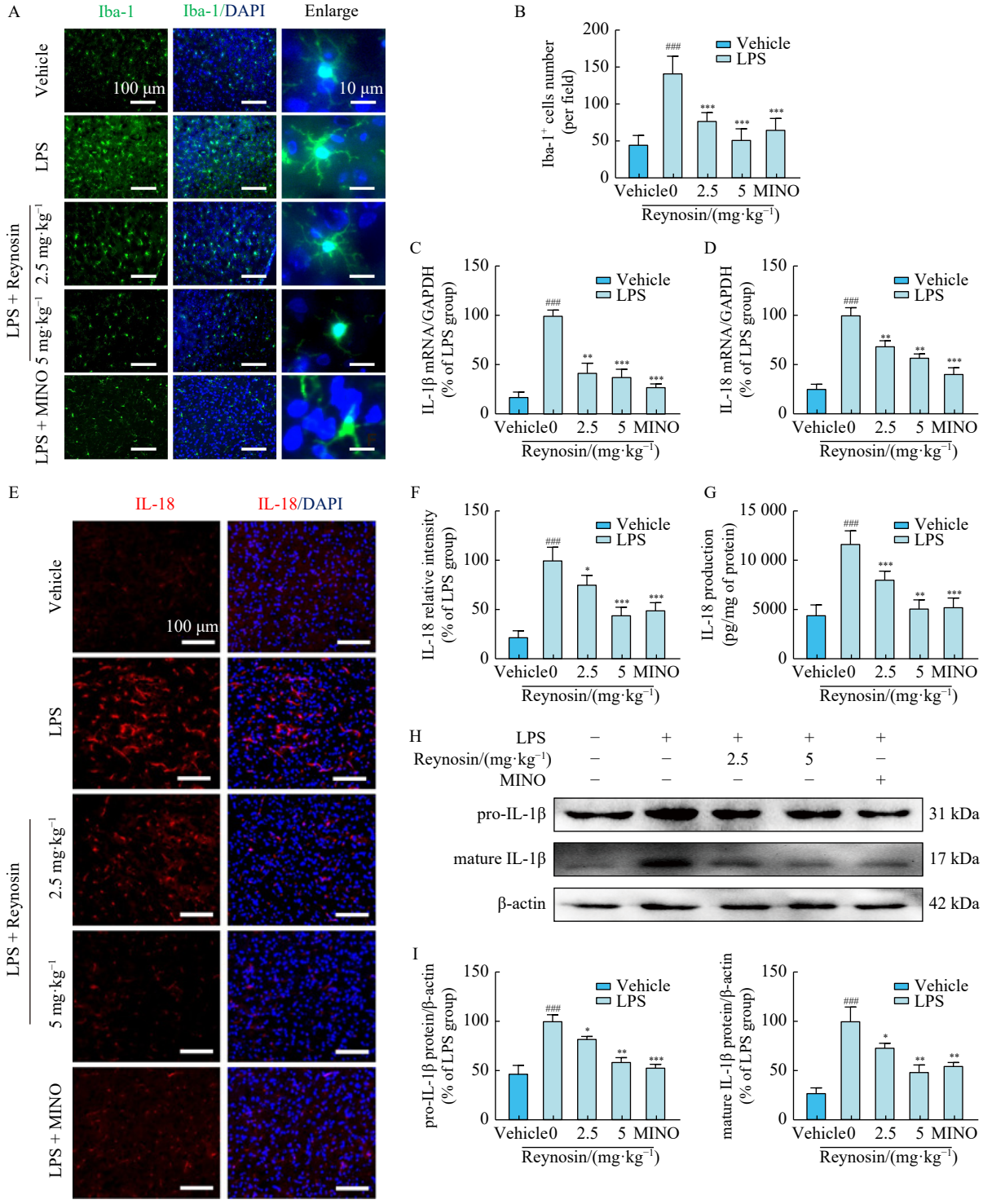

Fig. 2 Reynosin suppressed microglial inflammation activated by LPS *in vivo*. Mice were intracerebroventricularly injected with LPS to activate neuroinflammation *in vivo*. Microglial over-activation was evaluated using Iba-1 IF staining. (A–B) Representative images and statistical analysis of Iba-1 were shown (Iba-1: $n = 9$ from 3 mice, 100 × or 400 ×, scale bar = 100 μm or 10 μm). (C–D) IL-1β and IL-18 mRNA expressions were measured by RT-PCR, $n = 3$. IL-18 expression was assessed by immunofluorescence staining and an ELISA commercial kit. (E–F) Representative images of IL-18 staining and quantitative analysis were shown, $n = 5$. (G) The expression level of IL-18 was exhibited, $n = 6$ from 3 mice. The protein level of IL-1β was analyzed *via* Western blotting assay. (H–I) Representative images of pro-IL-1β and mature IL-1β immunoblot bands were presented, $n = 3$. Data are expressed as means ± SEM. $^{\#\#}P < 0.01$, $^{\#\#\#}P < 0.001$ *vs* the vehicle group; $^{*}P < 0.05$, $^{**}P < 0.01$ and $^{***}P < 0.001$ *vs* the LPS group. MINO: minocycline hydrochloride (40 mg·kg^{-1}).

Reynosin inhibits LPS-activated NLRP3 inflammasome activation in vitro and in vivo

To further elucidate the upstream regulatory mechanisms of reynosin, its effects on NLRP3 inflammasomes were investigated both *in vitro* and *in vivo*. In cell culture experiments, reynosin at concentrations of 1, 5, and 10 μmol·L^{-1} notably downregulated the transcriptional levels of NLRP3 and caspase-1, reduced NLRP3 protein expression, decreased caspase-1 self-cleavage, and diminished the number of ASC specks in LPS-treated BV-2 cells (Figs. 3A–3F). These effects were similarly observed with MINO, which served as a control (Figs. 3A–3F). In animal models, reynosin at doses of 2.5 and 5 mg·kg^{-1} effectively reduced the elevated mRNA levels of NLRP3 and caspase-1 induced by i.c.v. LPS injection (Fig. 3G–3H). Additionally, it significantly suppressed the upregulation of NLRP3 protein expression and caspase-1 self-cleavage observed following LPS treatment (Figs. 3I–3J). These *in vivo* findings are in agreement with the *in vitro* data, reinforcing the role of reynosin in mitigating NLRP3 inflammasome activation. The data also showed that MINO-treated samples exhibited lower levels of these inflammatory markers (Figs. 3G–3J).

Reynosin downregulates LPS-evoked ROS excessive release in vitro and in vivo

Reynosin was evaluated for its ability to modulate ROS generation following LPS induction both *in vitro* and *in vivo*. In cell-based assays, treatment with reynosin in LPS stimulated BV-2 cells, led to a decrease in DHE relative fluorescence intensity and reduced Amplex Red and H2DCFDA RFU, indicating a significant suppression of $O_2^{\cdot-}$, H_2O_2, and intracellular ROS levels (Figs. 4A–4D). Similar inhibitory effects on these oxidative stress markers were observed in cells treated with MINO (Figs. 4A–4D). *In vivo*, the application of reynosin to mice exposed to LPS significantly reduced oxidative stress markers in cortex tissues, as demonstrated by lower DHE relative fluorescence intensity, H_2O_2 content, and H2DCFDA RFU compared with those in LPS-administered mice (Figs. 4E–4H). These results indicate that reynosin effectively mitigates the accumulation of $O_2^{\cdot-}$, H_2O_2, and intracellular ROS that are typically elevated due to LPS-induced damage. MINO treatment also led to reduced levels of DHE fluorescence density, H_2O_2 content, and H2DCFDA RFU *in vivo*, further confirming the therapeutic potential of inhibiting ROS in the context of LPS-induced oxidative stress (Figs. 4E–4H).

Reynosin suppresses LPS-induced NADPH oxidase activation in vitro and in vivo

Reynosin was evaluated for its ability to suppress the activation of NADPH oxidase, a critical enzyme involved in ROS generation, both *in vitro* and *in vivo*. *In vitro*, after treatment with reynosin, LPS-stimulated BV-2 cells showed a significant reduction in the activation of NADPH oxidase, evidenced by downregulated levels of $NADP^+$ and NADPH, decreased mRNA and protein expression of $gp91^{phox}$, and reduced $p47^{phox}$ membrane translocation Figs. 5A–5D. Similarly, *in vivo* studies demonstrated that mice in the LPS group exhibited increased $NADP^+$ and NADPH levels, higher $gp91^{phox}$ mRNA and protein expressions, and more extensive $p47^{phox}$ membrane translocation compared with the vehicle group. Treatment with reynosin significantly mitigated these LPS-induced elevations, effectively inhibiting NADPH oxidase activity *in vivo* (Figs. 6A–6D). Reynosin treatment significantly suppressed these LPS-induced changes *in vivo* (Figs. 6A–6D). Moreover, MINO treatment also resulted in lowered levels of these indicators, further validating the potential of targeting NADPH oxidase in reducing oxidative stress and inflammation both *in vitro* (Figs. 5A–5D) and *in vivo* (Figs. 6A–6D).

Inhibition of NADPH oxidase enhances the effects of reynosin

To elucidate the inhibitory effects of reynosin on neuroinflammation *via* the reduction of NADPH oxidase-mediated NLRP3 inflammasome activation, BV-2 cells were pretreated with apocynin to inhibit NADPH oxidase and MCC950 to suppress the NLRP3 inflammasome. The results demonstrated that reynosin's inhibitory impact on $NADP^+$ and NADPH levels, as well as ROS production in LPS-activated BV-2 cells, was further enhanced when co-incubated with apocynin but not with MCC950, as depicted in Figs. 7A–7B. Notably, a more significant reduction in IL-1β and IL-18 mRNA expressions was observed in cells treated with both reynosin and apocynin compared with those treated with reynosin alone or reynosin with MCC950 (Figs. 7C–7D). Furthermore, the combined treatment with apocynin and MCC950 led to an additional decrease in IL-1β and IL-18 protein levels (Figs. 7E–7F). These findings confirm that reynosin effectively mitigates inflammatory responses by inhibiting the NADPH oxidase/NLRP3 inflammasome pathway.

Reynosin protects neuronal cells against microglial neuroinflammation in vitro and in vivo

Reynosin was evaluated for its neuroprotective properties against microglial-induced neuroinflammation in both *in vitro* and *in vivo* models. An *in vitro* CM culture model was utilized to assess the neurotoxic effects on SH-SY5Y neuronal cells, employing MTT, LDH assays, and calcein/PI staining. As displayed in Figs. 8A–8D, Results indicated that there were no significant changes in the viability of SH-SY5Y cells incubated with normal medium (blank group) or CM from the control group (CON-CM group), as evidenced by stable LDH levels and unchanged calcein and PI fluorescence intensities. However, when cells were exposed to CM from the LPS-stimulated group (LPS-CM group), there was a notable reduction in cell viability, increased LDH levels in the supernatant, decreased calcein fluorescence, and increased PI fluorescence, indicating enhanced neurotoxicity due to overactivated microglia. Importantly, these toxic effects were significantly mitigated by treatments with reynosin and MINO (Figs. 8A–8D). *In vivo* studies further supported these findings. Mice treated with LPS exhibited a reduction in NeuN-positive neuronal cells in the cortex compared with the

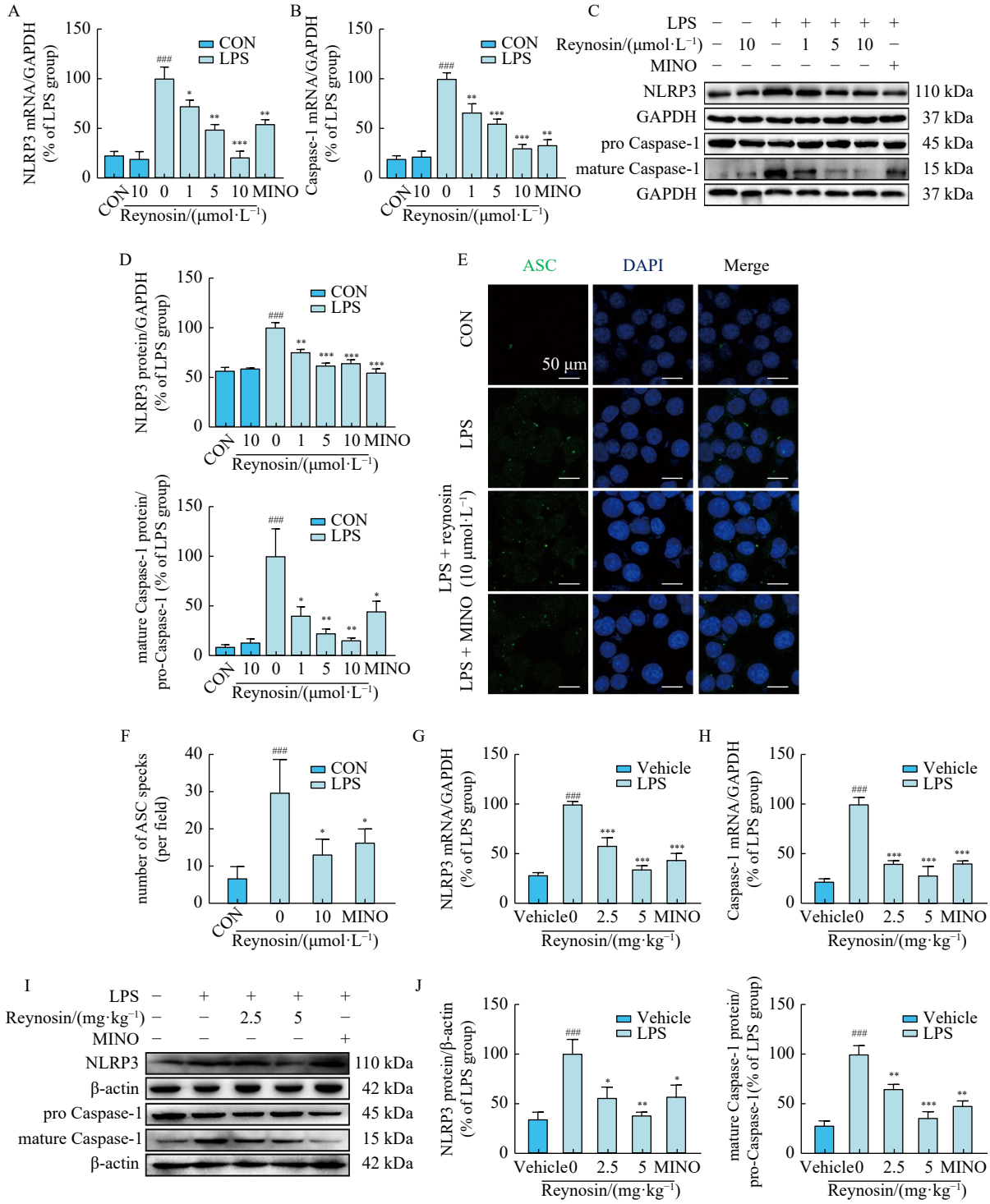

Fig. 3 Reynosin inhibited LPS-activated NLRP3 inflammasome *in vitro* and *in vivo*. (A–B, G–H) NLRP3 and caspase-1 mRNA expressions were measured using RT-PCR, $n = 3$. NLRP3 protein expression and caspase-1 cleavage were determined by Western blotting assay. (C–D, I–J) Representative immunoblot bands and quantitative analysis of NLRP3 and mature caspase-1 were shown, $n = 3$. ASC expression was measured by IF staining. (E–F) Representative images of ASC expression and quantitative analysis were displayed, $n = 4$, scale bar = 50 μm. Data are expressed as means ± SEM. $^{\#\#}P < 0.01$ and $^{\#\#\#}P < 0.001$ *vs* vehicle or CON group; $^{*}P < 0.05$, $^{**}P < 0.01$ and $^{***}P < 0.001$ *vs* LPS group. MINO: minocycline hydrochloride (30 μmol·L^{-1} for *in vitro*; 40 mg·kg^{-1} for *in vivo*).

vehicle group, suggesting neuronal loss associated with neuroinflammation. Conversely, treatment with reynosin and MINO effectively countered this loss, preserving NeuN-positive cells in the cortex (Figs. 8E–8F). These findings collectively demonstrate that reynosin not only mitigates microglial activation but also confers substantial neuroprotection against

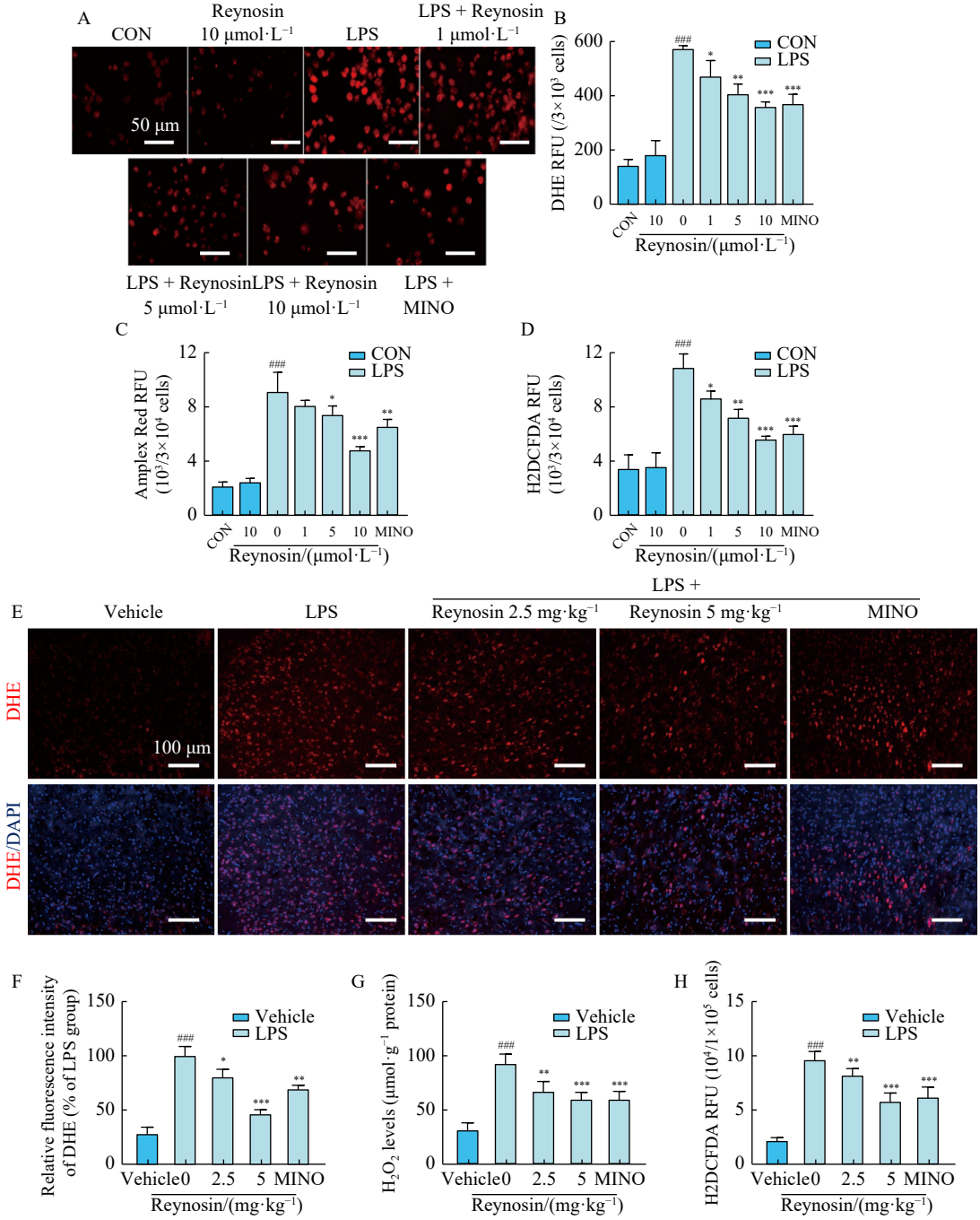

Fig. 4 Reynosin attenuated ROS over-accumulation induced by LPS *in vitro* and *in vivo*. The levels of superoxide anion were measured using DHE staining. (A–B, E–F) Typical pictures and statistical analysis of DHE staining were displayed, $n = 9$ from 3 mice; $n = 3$ from BV-2 cells, scale bar = 100 μm for mice and 50 μm for BV-2 cells. (C) H_2O_2 levels in BV-2 cells were measured by an Amplex Red commercial kit, $n = 3$. (G) The H_2O_2 contents in the cortex of mice were measured using a commercial kit, $n = 9$ from 3 mice. The levels of intracellular ROS were labeled with an H2DCFDA fluorescence probe. (D, H) Quantitative analysis of H2DCFDA fluorescence units were shown, $n = 9$ from 3 mice; $n = 3$ from BV-2 cells. Data are expressed as means ± SEM. $^{###}P < 0.001$ *vs* the CON or vehicle group; $^{*}P < 0.05$, $^{**}P < 0.01$ and $^{***}P < 0.001$ *vs* the LPS group. MINO: minocycline hydrochloride (30 μmol·L^{-1} for *in vitro*; 40 mg·kg^{-1} for *in vivo*).

the adverse effects of neuroinflammation.

Discussion

The current study has demonstrated that reynosin treatment provides significant neuroprotection against neuroinflammation both *in vivo* and *in vitro*. This protective effect is likely attributable to reynosin's ability to suppress NLRP3 inflammasome activation. Notably, this is the first report documenting the neuroinflammatory suppression mediated by reynosin in the brain, marking a significant contribution to

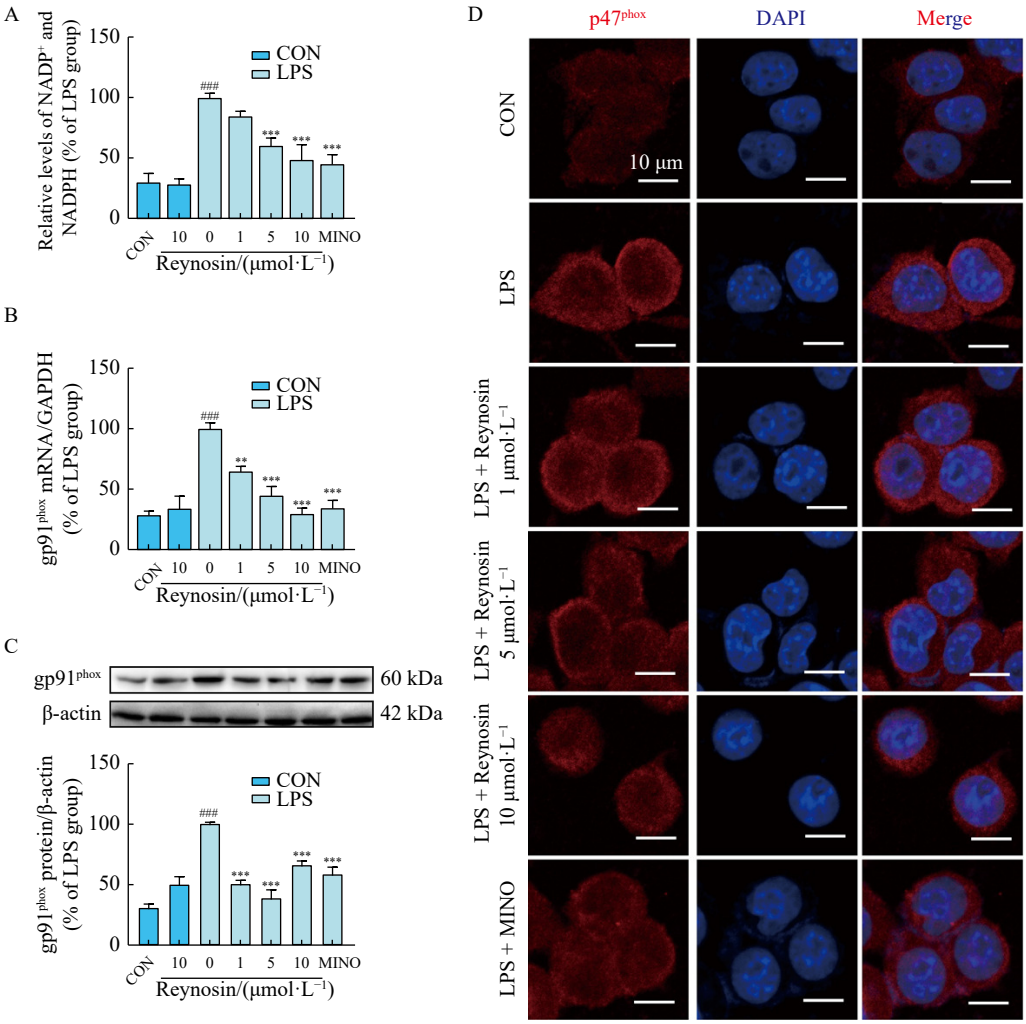

Fig. 5 Reynosin reduced NADPH oxidase activation stimulated by LPS *in vitro*. (A) Contents of intracellular $NADP^+$ and NADPH in the BV-2 cells were determined using a commercial kit, $n = 3$ from BV-2 cells. (B) The mRNA expression of $gp91^{phox}$ was measured using RT-PCR, $n = 3$. The protein expression of $gp91^{phox}$ was measured *via* Western blotting assay. (C) Representative immunoblot bands and quantitative analysis of $gp91^{phox}$ were displayed, $n = 3$. (D) The expression of $p47^{phox}$ in BV-2 cells was tested using IF staining, $n = 3$, scale bar = 10 μm for BV-2 cells. Data are expressed as means ± SEM, $^{###}P < 0.001$ *vs* the CON group; $^{***}P < 0.001$ *vs* the LPS group. MINO: minocycline hydrochloride (30 μmol·L^{-1}).

the existing literature on the pharmacological effects of reynosin. The findings presented herein highlight reynosin's potential as an effective inhibitor of neuroinflammation, offering promising therapeutic avenues for conditions characterized by neuroinflammatory processes. This study not only extends our understanding of reynosin's broad pharmacological profile but also underscores its therapeutic potential in combating NDDs.

Neuroinflammation is a multifaceted response, with microglia recognized as primary instigators of inflammatory processes in the brain [5, 10]. Upon activation, microglia release a plethora of inflammatory mediators that not only exacerbate local inflammation but also recruit adjacent immune cells, thereby contributing to neuronal degeneration and neurological impairments [7]. LPS, a component derived from the outer membrane of gram-negative bacteria, is widely used to induce neuroinflammation both *in vivo* and *in vitro* [34]. Exposure to LPS triggers elevated levels of pro-inflammatory cytokines, chemokines, nitric oxide, and ROS, along with abnormal activation of enzymes in cultured glial cells [34, 35]. Additionally, LPS exposure negatively impacts cultured neuronal cells by reducing cell viability [35], inducing nuclear condensation [35], causing synaptic loss and degenerative changes [36], and promoting abnormal aggregation of neurotoxic proteins such as amyloid-beta, tau, and alpha-synuclein [34, 36-38]. Intracerebral or systemic administration of LPS is known to activate microglia and astrocytes, trigger excessive release of pro-inflammatory cytokines or ROS [34], enhance processing and deposition of Aβ, α-synuclein [34, 38], and lead to significant neuronal loss [34]. These effects collectively result in memory deficits and behavioral alterations, making LPS a valuable tool for elucidating the connection between NDDs and central inflammation [34]. Our research reveals that reynosin effectively curtails microglial activation and signific-

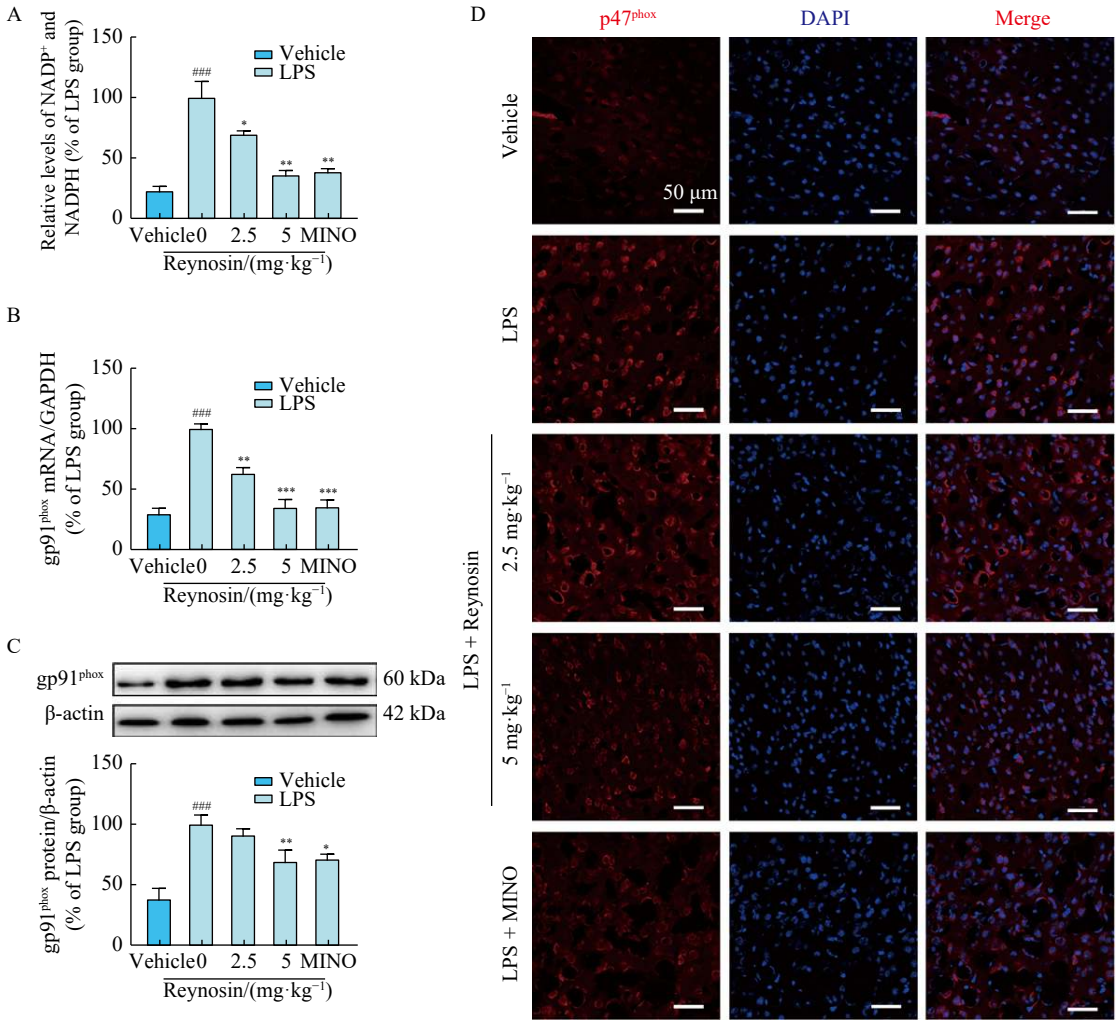

Fig. 6 Reynosin lowed NADPH oxidase activation activated by LPS *in vivo*. (A) Intracellular NADP$^+$ and NADPH in the cortex tissues were determined using a commercial kit, $n = 9$ from 3 mice. (B) The mRNA expression of gp91^{phox} was measured using RT-PCR, $n = 3$. The protein expression of gp91^{phox} was measured by Western blotting assay. (C) Typical immunoblot bands and quantitative analysis of gp91^{phox} were displayed, $n = 3$. (D) The expression of p47^{phox} in the cortex was measured by IF staining, $n = 3$, scale bar = 50 μm. Data are expressed as means ± SEM, $^{###}P < 0.001$ *vs* the vehicle group; $^{*}P < 0.05$, $^{**}P < 0.01$ and $^{***}P < 0.001$ *vs* the LPS group. MINO: minocycline hydrochloride (40 mg·kg^{-1}).

antly diminishes the production and release of the pro-inflammatory cytokines IL-1β and IL-18 in both LPS-stimulated cells and mice, thereby offering neuroprotection against LPS-induced damage. This study is the first to report reynosin's inhibitory effect on brain inflammation and provides novel evidence supporting its anti-inflammatory properties. These findings align with previous studies on its analog, Santamarin, which also demonstrated notable anti-inflammatory effects in LPS-activated macrophages [39]. Further, our *in vitro* assay showed that reynosin displays significant anti-inflammatory activity at concentrations lower than those of Santamarin. The differential activity may be attributed to variations in the substitution positions of the double bond within the reynosin molecule, which could affect its lipophilicity and molecular reactivity, enhancing its cellular membrane permeability and interaction with target proteins.

Numerous studies have shown that LPS can activate the NLRP3 inflammasome in microglia. LPS interacts with toll-like receptor 4 (TLR4), the most extensively studied of the TLRs, which is predominantly expressed on the surface of immune cells [34]. This interaction initiates the TLR4/MyD88/NF-κB signaling pathway [36], leading to the transcription of NLRP3 and caspase-1, as well as the transcription and translation of IL-1β and IL-18 [40]. The activation signals induced by LPS facilitate the assembly of the inflammasome complex, activation of caspase-1, and the catalytic processing of pro-IL-1β and pro-IL-18 into their active forms [12, 14, 16]. Additionally, LPS is involved in non-classical NLRP3 inflammasome activation by promoting pro-caspase-11 expression, which contributes to inflammasome-independent pyroptosis [41]. In this study, we report for the first time that reynosin attenuates NLRP3 inflammasome activation by inhibiting the transcription of NLRP3, caspase-1, IL-1β, and IL-18. Furthermore, reynosin suppresses NLRP3 protein ex-

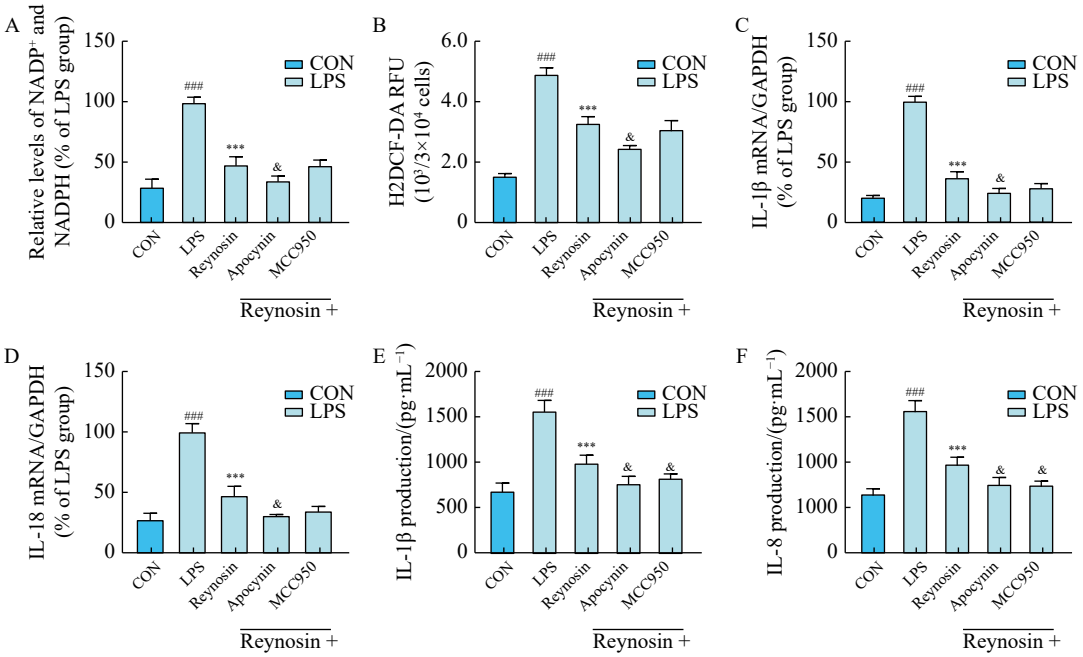

Fig. 7 The inhibition of NADPH oxidase activation enhanced the effects of reynosin on the expressions of ROS and pro-inflammatory cytokines. BV-2 cells were pre-treated with apocynin or MCC950 followed by reynosin incubation. (A) NADPH oxidase was evaluated by a commercial kit. (B) The intracellular ROS levels were measured using H2DCFDA staining. Real-time PCR (C–D) and ELISA (E–F) were performed to analyze the mRNA expressions and supernatant protein levels of IL-1β and IL-18. Data are expressed as means ± SEM. $^{\#\#\#}P < 0.001$ *vs* CON group, $^{***}P < 0.001$ *vs* LPS group, $^{\&}P < 0.05$ *vs* LPS + reynosin group.

pression, ASC oligomerization, caspase-1 activation, and the maturation and release of IL-1β and IL-18 in both LPS-activated mice and cell models. These findings underscore reynosin's potential as a therapeutic agent in managing inflammatory responses mediated by the NLRP3 inflammasome.

The dysregulated production of ROS is a key contributor to neuroinflammation in NDD brains due to the resulting oxidative stress. ROS also serve as upstream regulators that activate the NLRP3 inflammasome [21, 42], which is a common platform triggered by various endogenous and exogenous stimuli [42]. It is generally accepted that ROS are essential for the "priming" stage of NLRP3 inflammation [12, 42]. As a primary source of ROS, NADPH oxidase plays a crucial role in NLRP3 inflammasome activation [22]. In macrophages treated with NLRP3 agonists, both NLRP3 inflammasome activation and ROS production from NADPH oxidase are elevated [19, 43]. Inhibition of NADPH oxidase through genetic deletion of components like $gp91^{phox}$ or $p22^{phox}$ or pharmacological inhibition with apocynin or DPI reduces caspase-1 activation and IL-1β production [22, 40]. Yet, the necessity of ROS generated by NADPH oxidase during the NLRP3 inflammasome activation stage remains controversial. For example, macrophages from patients with chronic granulomatous disease (CGD) lacking $p22^{phox}$ still produce normal levels of IL-1β after stimulation with NLRP3 agonists [40], and caspase-1 activation in murine alveolar macrophages from $gp91^{phox-/-}$ mice remains unchanged after cyclic stretch [44]. These results revealed that NADPH oxidase is dispensable for the activation of the NLRP3 inflammasome and sparked the debate regarding whether ROS are truly involved in NLRP3 inflammasome activation but contribute to the priming stage. These findings suggest that NADPH oxidase might not be essential for NLRP3 inflammasome activation, stirring debate over ROS's role in this process and highlighting that ROS can be produced via various pathways, not exclusively through NADPH oxidase. In this study, we have discovered for the first time that reynosin effectively suppresses excessive intracellular ROS production, including $O_2^{\cdot-}$ and H_2O_2, by inhibiting the over-activation of NADPH oxidase. This suppression is evidenced by decreased $gp91^{phox}$ protein expression and prevention of $p47^{phox}$ membrane translocation. Moreover, cells co-treated with reynosin and the NADPH oxidase inhibitor apocynin exhibited reduced levels of ROS and pro-inflammatory cytokines IL-1β and IL-18. Furthermore, the cells co-treated with reynosin and NADPH oxidase inhibitor, apocynin, exhibited lower levels of ROS, IL-1β, and IL-18. However, co-incubation with reynosin and MCC950, the NLRP3 inflammasome inhibitor, did not exert suppressive effects on ROS and IL-1β and IL-18 mRNA expression. These findings suggest that reynosin's inhibition of the NLRP3 inflammasome activation is primarily mediated by suppressing NADPH oxidase over-activation. This mechanism represents a novel aspect of reynosin's anti-inflammatory effects and adds to our understanding of its potential therapeutic actions. While these findings are promising, there are limitations that merit consideration. Further investigation is needed to clarify the precise mechanisms by which reynosin inhibits NLRP3 inflammasome activation via attenuation of NADPH oxidase activity. Future studies will involve more targeted ap-

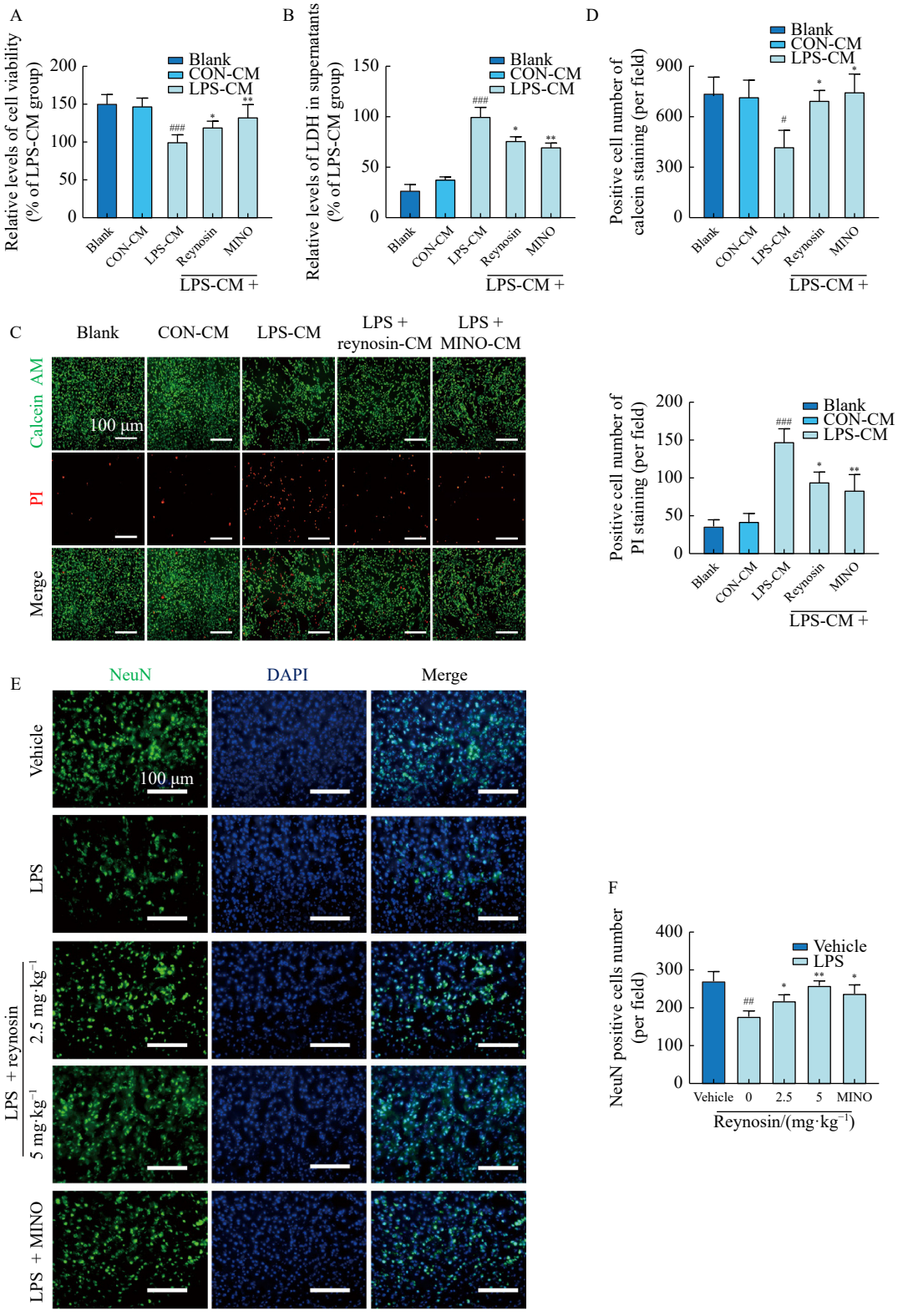

Fig. 8 Reynosin protected neurons from LPS damages *in vitro* and *in vivo*. *In vitro*, the cell viability of SH-SY5Y cells in CM model was measured using MTT assay (A), LDH commercial kit (B), and calcein AM/PI staining. (C–D) Representative images and statistical analysis of calcein AM and PI staining are shown, $n = 4$, scale bar = 100 μm. Neuronal loss in the cortex of mice was evaluated using NeuN IF staining. (E–F) Representative images and statistical analysis of NeuN staining were shown, $n = 9$ from 3 mice, scale bar = 100 μm. Data are expressed as means ± SEM. $^{\#}P < 0.05$, $^{\#\#}P < 0.01$, and $^{\#\#\#}P < 0.001$ *vs* the vehicle or CON-CM group, $^{*}P < 0.05$, and $^{**}P < 0.01$ *vs* the LPS or LPS-CM group. CM: conditional medium; MINO: minocycline hydrochloride (30 μmol·L^{-1} for *in vitro*; 40 mg·kg^{-1} for *in vivo*).

proaches, such as the use of small interfering RNA or short hairpin RNA, to delineate these pathways more clearly. Overall, reynosin demonstrates comprehensive inhibitory effects on multiple pathological processes involved in neuroinflammation, substantiating its potent neuroprotective capabilities even at low doses.

Conclusion

The present study conclusively demonstrates that reynosin exerts neuroprotective effects by mitigating microglial inflammation, primarily through the suppression of NLRP3 inflammasome activation. This suppression is facilitated by the inhibition of NADPH oxidase-mediated ROS production. Given these outcomes, reynosin emerges as a promising candidate for the treatment of NDDs characterized by the overactivation of the NLRP3 inflammasome. These findings not only enhance our understanding of reynosin's pharmacological profile but also underscore its potential utility in addressing a critical pathological mechanism in NDDs.

References

[1] Heemels MT. Neurodegenerative diseases [J]. *Nature*, 2016, **539**: 179.

[2] Dugger BN, Dickson DW. Pathology of neurodegenerative diseases [J]. *CSH Perspect Biol*, 2017, **9**(7): a028035.

[3] Jellinger KA. Basic mechanisms of neurodegeneration: a critical update [J]. *J Cell Mol Med*, 2010, **14**: 457-487.

[4] Peden AH, Ironside JW. Molecular pathology in neurodegenerative diseases [J]. *Curr Drug Targets*, 2012, **13**: 1548-1559.

[5] Kempuraj D, Thangavel R, Natteru PA, *et al*. Neuroinflammation induces neurodegeneration [J]. *J Neurol Neurosurg Spine*, 2016, **1**(1): 1003.

[6] Glass CK, Saijo K, Winner B, *et al*. Mechanisms underlying inflammation in neurodegeneration [J]. *Cell*, 2010, **140**: 918-934.

[7] Hickman S, Izzy S, Sen P, *et al*. Microglia in neurodegeneration [J]. *Nat Neurosci*, 2018, **21**: 1359-1369.

[8] ZhanY, Paolicelli RC, Sforazzini F, *et al*. Deficient neuron-microglia signaling results in impaired functional brain connectivity and social behavior [J]. *Nat Neurosci*, 2014, **17**: 400-406.

[9] Xu YL, Jiang CY, Wu JY, *et al*. Ketogenic diet ameliorates cognitive impairment and neuroinflammation in a mouse model of Alzheimer's disease [J]. *CNS Neurosci Ther*, 2022, **28**: 580-592.

[10] Mishra A, Bandopadhyay R, Singh PK, *et al*. Neuroinflammation in neurological disorders: pharmacotherapeutic targets from bench to bedside [J]. *Metab Brain Dis*, 2021, **36**: 1591-1626.

[11] Liston A, Masters SL. Homeostasis-altering molecular processes as mechanisms of inflammasome activation [J]. *Nat Rev Immunol*, 2017, **17**: 208-214.

[12] Kelley N, Jeltema D, Duan Y, *et al*. The NLRP3 Inflammasome: an overview of mechanisms of activation and regulation [J]. *Int J Mol Sci*, 2019, **20**: 3328.

[13] Lu A, Magupalli VG, Ruan J, *et al*. Unified polymerization mechanism for the assembly of ASC-dependent inflammasomes [J]. *Cell*, 2014, **156**: 1193-1206.

[14] Martinon F, Burns K, Tschopp J, *et al*. The inflammasome: a molecular platform triggering activation of inflammatory caspases and processing of pro IL-beta [J]. *Mol Cell*, 2002, **10**: 417-426.

[15] Fink SL, Cookson BT. Caspase-1-dependent pore formation during pyroptosis leads to osmotic lysis of infected host macrophages [J]. *Cell Microbiol*, 2006, **8**: 1812-1825.

[16] Anderson FL, Biggs KE, Rankin BE, *et al*. NLRP3 inflammasome in neurodegenerative disease [J]. *Transl Res*, 2023, **252**: 21-33.

[17] Saresella M, Rosa FL, Piancone F, *et al*. The NLRP3 and NLRP1 inflammasomes are activated in Alzheimer's disease [J]. *Mol Neurodegener*, 2016, **11**: 23.

[18] Heneka MT, Kummer MP, Stutz A, *et al*. NLRP3 is activated in Alzheimer's disease and contributes to pathology in APP/PS1 mice [J]. *Nature*, 2013, **493**: 674-678.

[19] Hewinson J, Moore SF, Glover C, *et al*. A key role for redox signaling in rapid P2X7 receptor-induced IL-1 beta processing in human monocytes [J]. *J Immunol*, 2008, **180**: 8410-8420.

[20] Brandes RP, Weissmann N, Schröder K. Nox family NADPH oxidases: molecular mechanisms of activation [J]. *Free Radic Biol Med*, 2014, **76**: 208-226.

[21] Bauernfeind F, Bartok E, Rieger A, *et al*. Cutting edge: reactive oxygen species inhibitors block priming, but not activation, of the NLRP3 inflammasome [J]. *J Immunol*, 2011, **187**: 613-617.

[22] Ma MW, Wang J, Dhandapani KM, *et al*. NADPH oxidase 2 regulates NLRP3 inflammasome activation in the brain after traumatic brain injury [J]. *Oxid Med Cell Longev*, 2017, **2**(017): 6057609.

[23] Qiu LL, Ji MH, Zhang H, *et al*. NADPH oxidase 2-derived reactive oxygen species in the hippocampus might contribute to microglial activation in postoperative cognitive dysfunction in aged mice [J]. *Brain Behav Immun*, 2016, **51**: 109-118.

[24] Shoaib M, Shah I, Ali N, *et al*. Sesquiterpene lactone! a promising antioxidant, anticancer and moderate antinociceptive agent from Artemisia macrocephala jacquem [J]. *BMC Complement Altern Med*, 2017, **17**(1): 27.

[25] Marino SD, Borbone N, Zollo F, *et al*. New sesquiterpene lactones from *Laurus nobilis* leaves as inhibitors of nitric oxide production [J]. *Planta Med*, 2005, **71**: 706-710.

[26] Garayev E, Herbette G, Giorgio CD, *et al*. New sesquiterpene acid and inositol derivatives from *Inula montana* L [J]. *Fitoterapia*, 2017, **120**: 79-84.

[27] Al-Attas AA, El-Shaer NS, Mohamed GA, *et al*. Anti-inflammatory sesquiterpenes from Costus speciosus rhizomes [J]. *J Ethnopharmacol*, 2015, **176**: 365-374.

[28] Lim S, Lee SJ, Nam KW, *et al*. Hepatoprotective effects of reynosin against thioacetamide-induced apoptosis in primary hepatocytes and mouse liver [J]. *Arch Pharm Res*, 2013, **36**: 484-494.

[29] Oh JH,Kim J, Karadeniz F, *et al*. Santamarine shows anti-photoaging properties via inhibition of MAPK/AP-1 and stimulation of TGF-β/Smad signaling in UVA-Irradiated HDFs [J]. *Molecules*, 2021, **26**: 3585.

[30] Ham A, Kim DW, Kim KH, *et al*. Reynosin protects against neuronal toxicity in dopamine-induced SH-SY5Y cells and 6-hydroxydopamine-lesioned rats as models of Parkinson's disease: reciprocal up-regulation of E6-AP and down-regulation of α-synuclein [J]. *Brain Res*, 2013, **1524**: 54-61.

[31] Zhu H, Jian ZH, Zhong Y, *et al*. Janus kinase inhibition ameliorates ischemic stroke injury and neuroinflammation through reducing NLRP3 inflammasome activation *via* JAK2/STAT3 pathway inhibition [J]. *Front Immunol*, 2021, **12**: 714943.

[32] Wang CY, Zhang Q, Xun Z, *et al*. Increases of iASPP-Keap1 interaction mediated by syringin enhance synaptic plasticity and rescue cognitive impairments *via* stabilizing Nrf2 in Alzheimer's models [J]. *Redox Biol*, 2020, **36**: 101672.

[33] Hu C, Zhang X, Wei WY, *et al*. Matrine attenuates oxidative stress and cardiomyocyte apoptosis in doxorubicin-induced car-

diotoxicity *via* maintaining AMPKα/UCP2 pathway [J]. *Acta Pharm Sin B*, 2019, **9**: 690-701.
[34] Batista CRA, Gomes GF, Candelario-Jalil E, *et al*. Lipopolysaccharide-induced induced neuroinflammation neuroinflammation as a bridge to understand neurodegeneration [J]. *Int J Mol Sci*, 2019, **20**: 2293.
[35] François A, Terro F, Janet T, *et al*. Involvement of interleukin-1β in the autophagic process of microglia: relevance to Alzheimer's disease [J]. *J Neuroinflammat*, 2013, **10**: 151.
[36] Yang XL, Zhang JD, Duan L, *et al*. Microglia activation mediated by toll-like receptor-4 impairs brain white matter tracts in rats [J]. *J Biomed Res*, 2018, **32**: 136-144.
[37] Zhang W, Gao JH, Yan ZF, *et al*. Minimally toxic dose of lipopolysaccharide and α-synuclein oligomer elicit synergistic dopaminergic neurodegeneration: role and mechanism of microglial NOX2 activation [J]. *Mol Neurobiol*, 2018, **55**: 619-632.
[38] Sheng JG, Bora SH, Xu G, *et al*. Lipopolysaccharide-induced-neuroinflammation increases intracellular accumulation of amyloid precursor protein and amyloid beta peptide in APPswe transgenic mice [J]. *Neurobiol Dis*, 2003, **14**: 133-145.
[39] Choi HG, Lee DS, Li B, *et al*. Santamarin, a sesquiterpene lactone isolated from *Saussurea lappa*, represses LPS-induced inflammatory responses *via* expression of heme oxygenase-1 in murine macrophage cells [J]. *Int Immunopharmacol*, 2012, **13**: 271-279.
[40] Liao PC, Chao LK, Chou JC, *et al*. Lipopolysaccharide/adenosine triphosphate-mediated signal transduction in the regulation of NLRP3 protein expression and caspase-1-mediated interleukin-1β secretion [J]. *Inflamm Res*, 2013, **62**: 89-96.
[41] Diamond CE, Khameneh HJ, Brough D, *et al*. Novel perspectives on non-canonical inflammasome activation [J]. *Immunotargets Ther*, 2015, **4**: 131-141.
[42] Abais JM, Xia M, Zhang Y, *et al*. Redox regulation of NLRP3 inflammasomes: ROS as trigger or effector? [J]. *Antioxid Redox Signal*, 2015, **22**: 1111-1129.
[43] Cruz CM, Rinna A, Forman HJ, *et al*. ATP activates a reactive oxygen species-dependent oxidative stress response and secretion of proinflammatory cytokines in macrophages [J]. *J Biol Chem*, 2007, **282**: 2871-2879.
[44] Wu JB, Yan Z, Schwartz DE, *et al*. Activation of NLRP3 inflammasome in alveolar macrophages contributes to mechanical stretch-induced lung inflammation and injury [J]. *J Immunol*, 2013, **190**: 3590-3599.

Cite this article as: YANG Yanqiu, CHE Yue, FANG Mingxia, *et al*. Reynosin protects neuronal cells from microglial neuroinflammation by suppressing NLRP3 inflammasome activation mediated by NADPH oxidase [J]. *Chin J Nat Med*, 2024, **22**(6): 486-500.

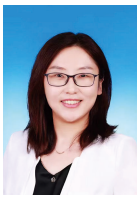

Professor Li Ning has been selected for the national-level young talent, the young top talent of "Xingliao Talent Plan", and the hundred-level talent of Liaoning province. She is currently the dean of School of Traditional Chinese Materia Medica, deputy director of the Key Laboratory of "Target-based Drug Design and Research" of Ministry of Education, and director of the Key Laboratory of Innovative Traditional Chinese Medicine for Major Chronic Diseases of Liaoning Province. She focuses on studies regarding preventing and treating major diseases with Traditional Chinese Medicine. She has presided over 8 National Natural Science Foundation projects. As the first/corresponding author, she has published 126 SCI papers, obtained 32 authorized invention patents, and wrote 22 monographs (5 in English). She won 2011' CPA-Servier Young Investigator Awards in Medicinal Chemistry and three provincial Science and Technology Progress Awards. She is also the youth Committee member of the Chinese Society of Traditional Chinese Medicine and the vice Chairman of the Chinese Medicine Chemistry Branch.

Prof. Hou Yue is the director of Key Laboratory of Bioresource Research and Development of Liaoning Province. She received her B.E. degree in 2000 and Ph.D. degree in 2005 from Shenyang Pharmaceutical University. She is mainly engaged in research on the effect and mechanism of natural constituent from Chinese herbal medicine or plants against stroke and Alzheimer's disease. To date, she has published over 100 SCI papers, including Advanced Science, Phytomedicine, Journal of Neuroinflammation, etc.